

Lanthanide-containing Peroxoisopolytungstate with Tetrahedral WO_4^{2-} Template Core, $[\text{Ln}_4(\text{WO}_4)(\text{H}_2\text{O})_{16}\{\text{W}_7\text{O}_{22}(\text{O}_2)_2\}_4]^{14-}$

Lanying Song, Dongdi Zhang, Pengtao Ma, Zhijie Liang, Jingping Wang* and Jingyang Niu*

Henan Key Laboratory of Polyoxometalate, Institute of Molecular and Crystal Engineering, College of Chemistry and Chemical Engineering, Henan University, Kaifeng, Henan 475004 (China), Fax: (+86) 378-3886876; E-mail: jyniu@henu.edu.cn ; jpwang@henu.edu.cn

Supporting information

Fig. S1 The coordination environments of La and W8

Fig. S2 Schematic presentation of the anion $[\text{Ln}_4(\text{WO}_4)(\text{H}_2\text{O})_{16}\{\text{W}_7\text{O}_{22}(\text{O}_2)_2\}_4]^{14-}$

Fig. S3 $(3^4 \cdot 4^{12} \cdot 5^{11} \cdot 6)$ topology framework of **1**.

Fig. S4 Charge distribution of O atoms in **1a**

Fig. S5 Charge distribution of O atoms in **2a**

Fig. S6 TG curves of **1** (left) and **2** (right)

Fig. S7 ^{183}W NMR spectra of **1**

Fig. S8 The negative-mode ESI mass spectrum in water solution of **1**

Fig. S9 An expansion of the peaks at m/z 248.9364 (HWO_4^-) and at m/z 280.9297 ($[\text{W}^{\text{VI}}\text{O}(\text{O}_2)_2(\text{OH})]^-$) are shown along with the calculated isotopic pattern (red columns) of **1a**.

Fig. S10 An expansion of the peaks at m/z 701.7982 ($[\text{La}(\text{W}^{\text{V}}_2\text{W}^{\text{VI}}_3\text{O}_{17})(\text{H}_2\text{O})_4\text{H}]^{2-}$) and at m/z 710.8072 ($[\text{La}(\text{W}^{\text{V}}_2\text{W}^{\text{VI}}_3\text{O}_{17})(\text{H}_2\text{O})_5\text{H}]^{2-}$) are shown along with the calculated isotopic pattern (red columns) of **1a**.

Fig. S11 The negative-mode ESI mass spectrum in water solution of **2**

Fig. S12 An expansion of the peaks at m/z 248.9358 (HWO_4^-) and at m/z 280.9271 ($[\text{W}^{\text{VI}}\text{O}(\text{O}_2)_2(\text{OH})]^-$) are shown along with the calculated isotopic pattern (red columns) of **2a**.

Fig. S13 An expansion of the peaks at m/z 702.7990 ($[\text{Pr}(\text{W}^{\text{V}}_2\text{W}^{\text{VI}}_3\text{O}_{17})(\text{H}_2\text{O})_4\text{H}]^{2-}$) and at m/z 711.8051 ($[\text{Pr}(\text{W}^{\text{V}}_2\text{W}^{\text{VI}}_3\text{O}_{17})(\text{H}_2\text{O})_5\text{H}]^{2-}$) are shown along with the calculated isotopic pattern (red columns) of **2a**.

Fig. S14 IR spectra of **1** and **2**

Fig. S15 IR spectra of $[(t\text{-C}_4\text{H}_9)\text{NH}_3]_6[\text{W}_7\text{O}_{24}] \cdot 2\text{H}_2\text{O}$ and **2**

Fig. S16 The simulated and experimental powder XRPD patterns: **1** (left), **2** (right)

Table S1 The bond valence sum calculations of all the oxygen atoms on polyanion in **1a**

Table S2 The bond valence sum range of all the oxygen atoms on polyanion in **1a**

Table S3 The bond valence sum calculations of W and La in **1a**

Table S4 The bond valence sum calculations of all the oxygen atoms on polyanion in **2a**

Table S5 The bond valence sum range of all the oxygen atoms on polyanion in **2a**

Table S6 The bond valence sum calculations of W and Pr in **2a**

Table S7 Calculated isotopic pattern of HWO_4^- (m/z 248.9364)

Table S8 Calculated isotopic pattern of $[\text{W}^{\text{VI}}\text{O}(\text{O}_2)_2(\text{OH})]^-$ (m/z 280.9297)

Table S9. Calculated isotopic pattern of $[\text{La}(\text{W}^{\text{V}}_2\text{W}^{\text{VI}}_3\text{O}_{17})(\text{H}_2\text{O})_4\text{H}]^{2-}$ (m/z 701.7982)

Table S10. Calculated isotopic pattern of $[\text{La}(\text{W}^{\text{V}}_2\text{W}^{\text{VI}}_3\text{O}_{17})(\text{H}_2\text{O})_5\text{H}]^{2-}$ (m/z 710.8072)

Table S11. Calculated isotopic pattern of $[\text{Pr}(\text{W}^{\text{V}}_2\text{W}^{\text{VI}}_3\text{O}_{17})(\text{H}_2\text{O})_4\text{H}]^{2-}$ (m/z 702.7990)

Table S12. Calculated isotopic pattern of $[\text{Pr}(\text{W}^{\text{V}}_2\text{W}^{\text{VI}}_3\text{O}_{17})(\text{H}_2\text{O})_5\text{H}]^{2-}$ (m/z 711.8051)

Physical measurements

All chemical materials were purchased from commercial sources and used without further purification. Elemental analyses (C, H and N) were conducted on a Perkin-Elmer 2400-II CHNS/O analyzer. Inductively coupled plasma (ICP) analyses were performed on a Perkin-Elmer Optima 2000 ICP-OES spectrometer. IR spectra were recorded on a Bruker VERTEX 70 spectrometer using KBr pellets in the range of 4000–400 cm^{-1} . X-ray powder diffraction (XRPD) were performed on a Philips X'Pert-MPD instrument with Cu $K\alpha$ radiation ($\lambda = 1.54056 \text{ \AA}$) in the range $2\theta = 10 - 40^\circ \text{C}$ at 293 K. TG analyses were performed under N_2 atmosphere on a Mettler–Toledo TGA/SDTA851^e instrument with the heating rate of 10 $^\circ\text{C min}^{-1}$ from 25 to 800 $^\circ\text{C}$.

Synthesis of $\text{K}_6\text{Na}_4[\text{H}_{32}\{\text{Pr}_4(\text{WO}_4)(\text{H}_2\text{O})_{16}[\text{W}_7\text{O}_{22}(\text{O}_2)_2]_4\}_3] \cdot \text{ca}105\text{H}_2\text{O}$ (**2**)

The synthetic procedure for **2** was the same as for **1** except that $\text{Pr}(\text{NO}_3)_3 \cdot 6\text{H}_2\text{O}$ (0.073 g, 0.17mmol) was used instead of $\text{La}(\text{NO}_3)_3 \cdot 6\text{H}_2\text{O}$. Yield: ca. 0.21 g, 57% (based on $\text{Pr}(\text{NO}_3)_3 \cdot 6\text{H}_2\text{O}$). Anal.calcd. (%) for **2**: H 1.31, Na 0.35, K 0.90, Pr 6.51, W 61.55; found: H 1.35, Na 0.40, K 0.98, Pr 6.45, W 61.45. IR (KBr pellet): 3434(s), 1631(s), 1385(w), 964(s), 945(w), 904(s), 844(m), 738(w), 687(w), 649(s), 602(w), 557(m), 493(m).

These polyanions were synthesized by the reaction of Na_2WO_4 and lanthanide salts in acidic aqueous medium. The ratio of WO_4^{2-} and Ln^{3+} , pH and temperature are essential to successful synthesis of **2**. The inserted amounts of lanthanide ions in relation to tungstate are not stoichiometric and vary from 10:1 to 30:1 resulted in a successful synthetic procedure, with ratio in about 16:1 being suitable for X-ray diffraction. A pH window of 2.5–3.5 resulted in a successful synthetic procedure, with pH 3.0 being optimal. A pH lower than 2.5 provide white precipitate without any product, and a pH higher than 3.7 gave the colourless and blocky paradodecatungstate $[\text{H}_2\text{W}_{12}\text{O}_{42}]^{10-}$ as the main product. Also, the temperature of the reaction solution affects the formation and yield of polyanions. The polyanions were formed at room temperature as well as at 60 $^\circ\text{C}$, but resulted in a higher yield at 60 $^\circ\text{C}$. If the synthesis solution of **2** is heated to 70 $^\circ\text{C}$ -80 $^\circ\text{C}$, the well-known metatungstate ion $[\text{H}_2\text{W}_{12}\text{O}_{40}]^{10-}$ is formed. Also, the pH value of heated resulting solution change became 5.6 from 2.4. In addition, the amounts of H_2O_2 are essential to successful synthesis. The optimal amount of 30% H_2O_2 is about 2ml for reaction system, which can yield good crystals suitable for X-ray diffraction. Change in the amount of H_2O_2 could bring about a change in the pH value, leading to snowflake crystals or precipitate.

X-ray Crystallography

Intensity data for **1** and **2** were collected at 296 K on a Bruker APEX-II CCD diffractometer using graphite-monochromated Mo $K\alpha$ radiation ($\lambda = 0.71073 \text{ \AA}$). Routine Lorentz and polarization corrections were applied and an absorption correction was performed using the SADABS program. Direct methods were used to solve the structure and refined by full-matrix least-squares on F^2 using the SHELXTL-97 program package. All non-hydrogen atoms were refined anisotropically. Further details on the crystal structure investigation may be obtained from the

Fachinformationszentrum Karlsruhe, 76344 Eggenstein-Leopoldshafen, Germany (fax: (+49)7247-808-666; e-mail: crysdata@fiz-karlsruhe.de), on quoting the depository numbers CSD-425725 (**1**), CSD-425726 (**2**), respectively.

Crystal data for **1**, $\text{H}_{338}\text{K}_6\text{La}_{12}\text{Na}_4\text{O}_{477}\text{W}_{87}$, $M_r = 25959.89$, cubic, $a = b = c = 36.253(5) \text{ \AA}$, $\alpha = \beta = \gamma = 90^\circ$, $V = 47648(11) \text{ \AA}^3$, $T = 296(2) \text{ K}$, space group I-43d, $Z = 4$, $D_c = 3.44613 \text{ g cm}^{-3}$, $\mu = 22.106 \text{ mm}^{-1}$, $F(000) = 42928$, $GOF = 1.074$. A total of 117151 reflections were collected, 6996 of which were unique ($R_{\text{int}} = 0.1061$). $R_1(wR_2) = 0.0413(0.1064)$ for 406 parameters and 6996 reflections ($I > 2\sigma(I)$).

Crystal data for **2**, $\text{H}_{338}\text{K}_6\text{Pr}_{12}\text{Na}_4\text{O}_{477}\text{W}_{87}$, $M_r = 25983.92$, cubic, $a = b = c = 36.028(9) \text{ \AA}$, $\alpha = \beta = \gamma = 90^\circ$, $V = 46748(5) \text{ \AA}^3$, $T = 296(2) \text{ K}$, space group I-43d, $Z = 4$, $D_c = 3.535 \text{ g cm}^{-3}$, $\mu = 22.712 \text{ mm}^{-1}$, $F(000) = 43272$, $GOF = 1.059$. A total of 113980 reflections were collected, 6865 of which were unique ($R_{\text{int}} = 0.0976$). $R_1(wR_2) = 0.0363(0.0896)$ for 406 parameters and 6865 reflections ($I > 2\sigma(I)$).

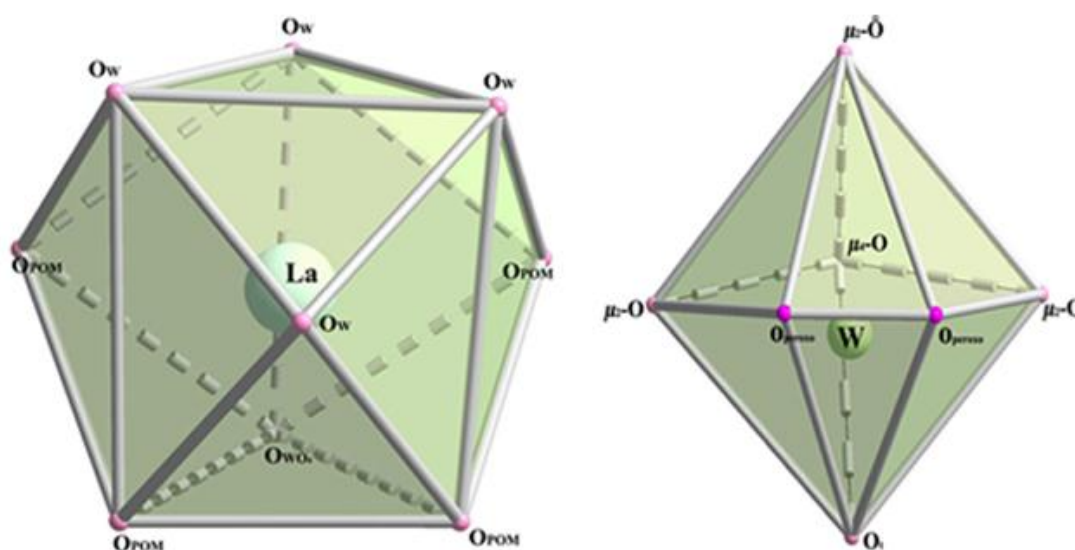


Fig. S1 The coordination environments of La (left) and W_8 (right)

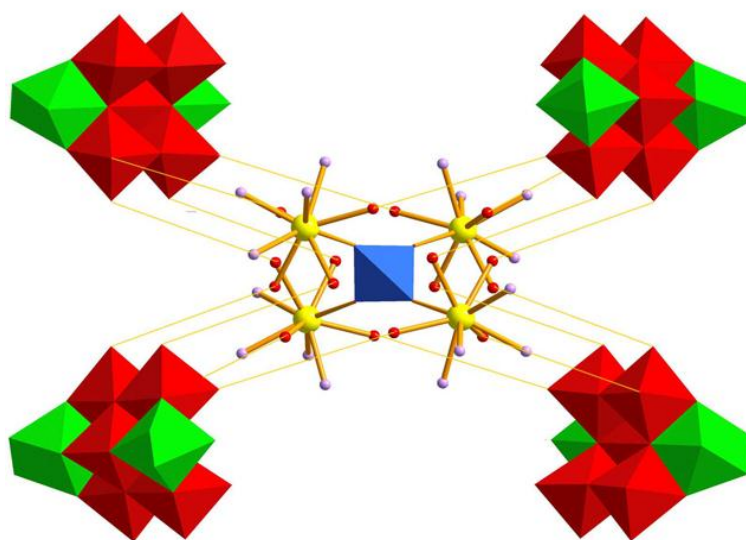


Fig. S2 Schematic presentation of the anion $[\text{Ln}_4(\text{WO}_4)(\text{H}_2\text{O})_{16}\{\text{W}_7\text{O}_{22}(\text{O}_2)_2\}_4]^{14-}$

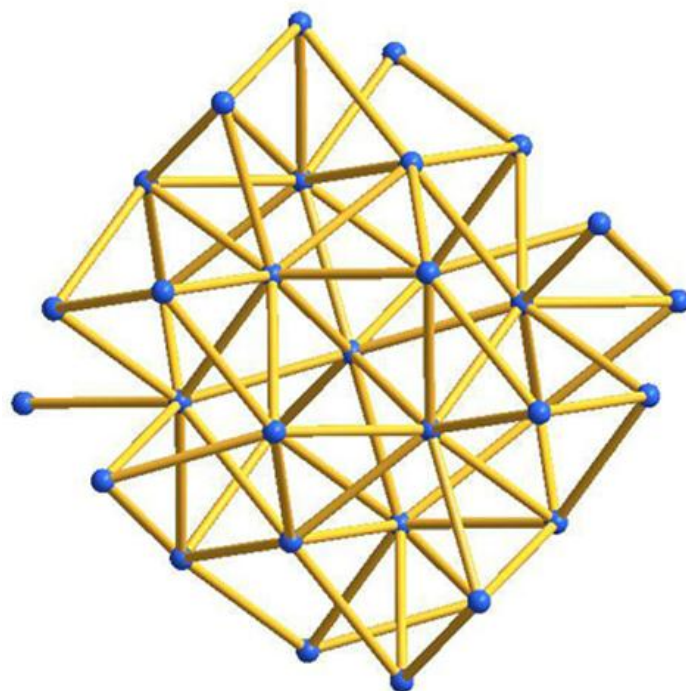


Fig. S3 $(3^4 \cdot 4^{12} \cdot 5^{11} \cdot 6)$ topology framework of **1**

Bond valence sum calculations for $[\text{La}_4(\text{WO}_4)(\text{H}_2\text{O})_{16}\{\text{W}_7\text{O}_{22}(\text{O}_2)_{24}\}]^{14-}$ and $[\text{Pr}_4(\text{WO}_4)(\text{H}_2\text{O})_{16}\{\text{W}_7\text{O}_{22}(\text{O}_2)_{24}\}]^{14-}$

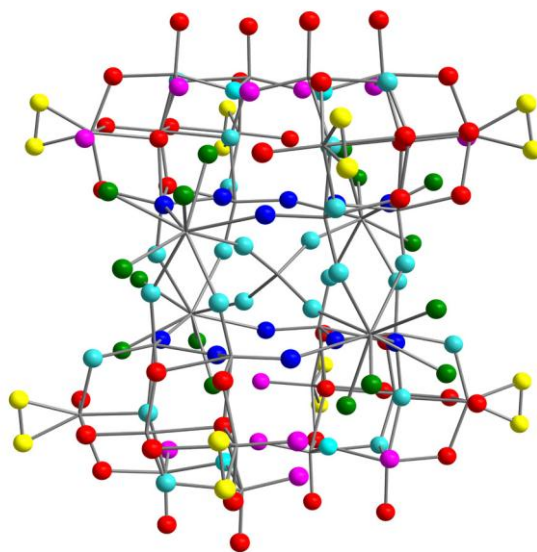


Fig. S4 Charge distribution of O atoms in **1a**. Oxygen atoms with different, bond valence sums are represented by different colours.

Table S1 The bond valence sum calculations of all the oxygen atoms on polyanion **1a**

Atom	Bond valence sum	Atom	Bond valence sum	Atom	Bond valence sum
O1	1.99	O12, O22	1.75	O17	0.97
O2	1.96	O13, O15	1.80	O18	1.04
O3	2.04	O14	1.90	O26	0.99
O4, O9	2.00	O16	1.84	O27	0.97

O5	1.89	O19	1.58	O1W	0.25
O6	1.93	O20	1.71	O2W	0.33
O7	1.92	O21	1.94	O3W	0.36
O8	1.98	O23	1.67	O4W	0.34
O10	1.85	O24	1.79		
O11	1.87	O25	1.65		

Table S2 The bond valence sum range of all the oxygen atoms on polyanion **1a**







Oxygen atom	Bond valence sum range	Number	Oxygen atom	Bond valence sum range	Number
	-2.1 ~ -2.0	12		-1.7 ~ -1.5	12
	-2.0 ~ -1.9	28		-1.2 ~ -0.9	16
	-1.9 ~ -1.7	40		-0.50 ~ -0.00	16

Table S3. The bond valence sum calculations of W and La in **1a**

Atom lable	Calc. For W(VI)
W(1)	5.76
W(2)	6.12
W(3)	6.08
W(4)	5.92
W(5)	6.43
W(6)	6.02
W(7)	6.03
W(8)	6.19
Atom lable	Calc. For La(III)
La(1)	3.19

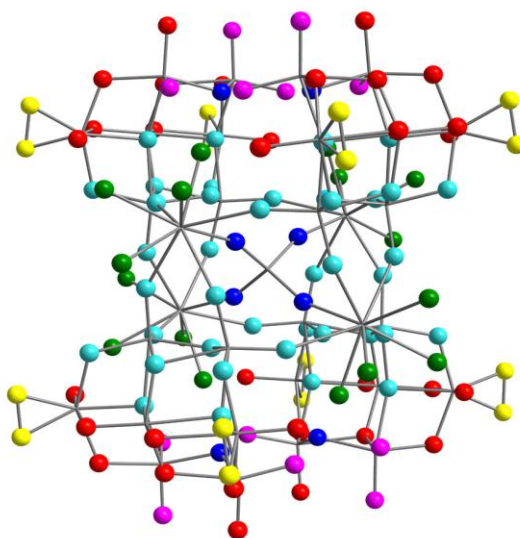


Fig. S5 Charge distribution of O atoms in **2a**. Oxygen atoms with different, bond valence sums are represented by different colours.

Table S4 The bond valence sum calculations of all the oxygen atoms on polyanion in **2a**

Atom	Bond valence sum	Atom	Bond valence sum	Atom	Bond valence sum
O1	2.07	O13	1.81	O25	1.71
O2, O6, O9	1.94	O14	1.89	O17	1.10
O3	1.95	O15	1.78	O18	1.19
O4	1.98	O16	1.82	O26	0.96
O5	1.91	O19	1.66	O27	0.99
O7	1.96	O20	1.60	O1W	0.24
O8	1.99	O21	2.00	O2W	0.33
O10	1.90	O22	1.75	O3W	0.34
O11	1.93	O23	1.61	O4W	0.34
O12	1.85	O24	1.84		

Table S5 The bond valence sum range of all the oxygen atoms on polyanion in **2a**







Oxygen atom	Bond valence sum range	Number	Oxygen atom	Bond valence sum range	Number
	-2.1 ~ -2.0	8		-1.7 ~ -1.5	12
	-2.0 ~ -1.9	40		-1.2 ~ -0.9	16
	-1.9 ~ -1.7	32		-0.56 ~ -0.00	16

Table S6. The bond valence sum calculations of W and Pr in **2a**

Atom lable	Calc. For W(VI)
W(1)	6.16
W(2)	5.95
W(3)	6.07
W(4)	6.00
W(5)	6.26
W(6)	6.00
W(7)	5.99
W(8)	6.20
Atom lable	Calc. For Pr(III)
Pr(1)	3.28

To balance the charges of **1** and **2**, thirty-two protons should be added, respectively. These protons cannot be located crystallographically and are assumed to be delocalized over the entire structures, which is common in polyoxometalates. The multiply protonated polyoxotungstate fragments in both compounds are reasonable. The reasons are as follows: a) The polyanions $[\text{La}_4(\text{WO}_4)(\text{H}_2\text{O})_{16}\{\text{W}_7\text{O}_{22}(\text{O}_2)_2\}_4]^{14-}$ in **1** and $[\text{Pr}_4(\text{WO}_4)(\text{H}_2\text{O})_{16}\{\text{W}_7\text{O}_{22}(\text{O}_2)_2\}_4]^{14-}$ in **2** have high negative charges and rich basic surface oxygen atoms, which make these POM fragments readily protonated; b) On the basis of valence sum (Σ_s) calculations, the oxidation states 124 O atoms in $[\text{Ln}_4(\text{WO}_4)(\text{H}_2\text{O})_{16}\{\text{W}_7\text{O}_{22}(\text{O}_2)_2\}_4]^{14-}$ of **1** and **2** can be divided into six groups according to their bond valence sums (Table S1-S6). For **1a**, except that eight O-O groups ($\Sigma_s = -1.2 \sim -0.9$) and sixteen H_2O ($\Sigma_s = -0.50 \sim -0.00$) groups, there are forty O atoms with their Σ_s in the range of $-1.9 \sim -1.7$ and even twelve O atoms with their Σ_s in the range of $-1.7 \sim -1.5$. So protons are likely to be delocalized

on these O atoms, especially the twelve O atoms with their Σ_s in the range of $-1.5 \sim -1.7$; For **2a**, except that eight O-O groups ($\Sigma_s = -1.2 \sim -0.9$) and sixteen H₂O ($\Sigma_s = -0.50 \sim -0.00$) groups, there are thirty-two O atoms with their Σ_s in the range of $-1.9 \sim -1.7$ and even twelve O atoms with their Σ_s in the range of $-1.7 \sim -1.5$. So protons are likely to be delocalized on these O atoms, especially the twelve O atoms with their Σ_s in the range of $-1.7 \sim -1.5$; c) In generally, the multiply protons can not be located in polyoxometalates units by X-ray diffraction, and they are usually assigned to be delocalized on the whole POM only for balancing the high negative charges of the polyoxoanion, which is common in POM chemistry, for example, [H₁₂V₁₃O₄₀]³⁻,¹ [H₃W₁₂O₄₀]⁵⁻,² [H₆Ni₂₀P₄W₃₄(OH)₄O₁₃₆(enMe)₈(H₂O)₆]⁶⁻ and [H₈Ni₂₀P₄W₃₄(OH)₄O₁₃₆(en)₉(H₂O)₄]⁴⁻,³ [Sn₄(SiW₉O₃₄)₂]¹²⁻,⁴ [(H₃O)₉{(PY₂W₁₀O₃₈)₄(W₃O₁₄)}]²¹⁻ and [(H₃O)_{13.5}{(PEu₂W₁₀O₃₈)₄(W₃O₁₄)}]^{16.5-},⁵ [HW₉O₃₃Ru^{II}₂(dmsO)₆]⁷⁻,⁶ [H₂₃NaO₈Cu₂₄(Nb₇O₂₂)₈]¹⁶⁻ and [H₉Cu_{25.5}O₈(Nb₇O₂₂)₈]²⁸⁻.⁷

TG curves

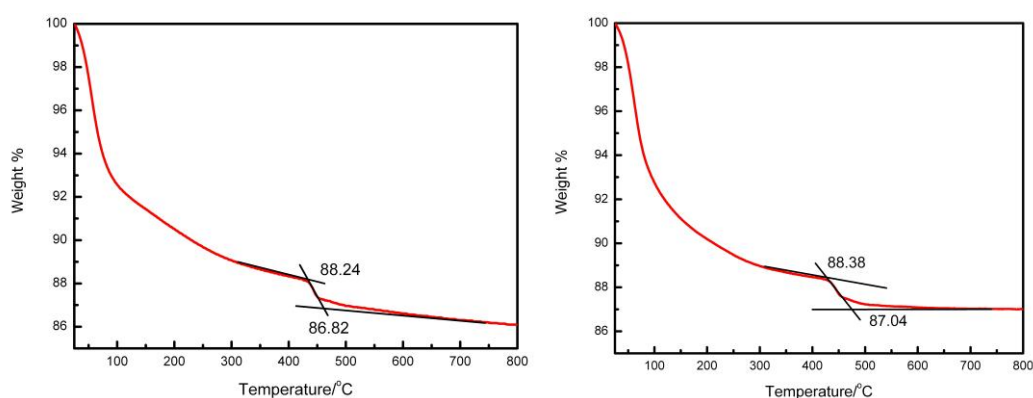


Fig. S6 TG curves of **1** (left) and **2** (right) measured in the range of 25–800 °C under nitrogen gas atmosphere with the heating rate of 10 °C/min.

Thermal gravimetric analyses (TGA) were performed under N₂ atmosphere from 25 to 800 °C (Fig. S6). The TG processes of **1** and **2** are very similar. In the case of **1**, a weight loss of 11.76% was observed in the range of 25–430 °C, attributing to the removal of about 105 crystal water molecules, 48 coordinated water molecules and the dehydration of 32 protons.; calcd. 11.72% for $x \approx 105$ in K₆Na₄[H₃₂{La^{III}₄(WO₄)(H₂O)₁₆[W₇O₂₂(O₂)₂]₄}₃].xH₂O. A weight loss of 1.42% observed from 430 °C up to ca. 460 °C is due to loss of one oxygen atom in each peroxy group (calcd. 1.48%). In the case of **2**, a weight loss of 11.62% was observed in the range of 25–435 °C, attributing to the removal of about 105 crystal water molecules, 48 coordinated water molecules and the dehydration of 32 protons; calcd. 11.70% for $y \approx 105$ in K₆Na₄[H₃₂{Pr^{III}₄(WO₄)(H₂O)₁₆[W₇O₂₂(O₂)₂]₄}₃].yH₂O. A weight loss of 1.36% observed from 435 °C up to ca. 480 °C is due to decomposition of one oxygen atom in each peroxy group (calcd. 1.47%).

¹⁸³W NMR spectra

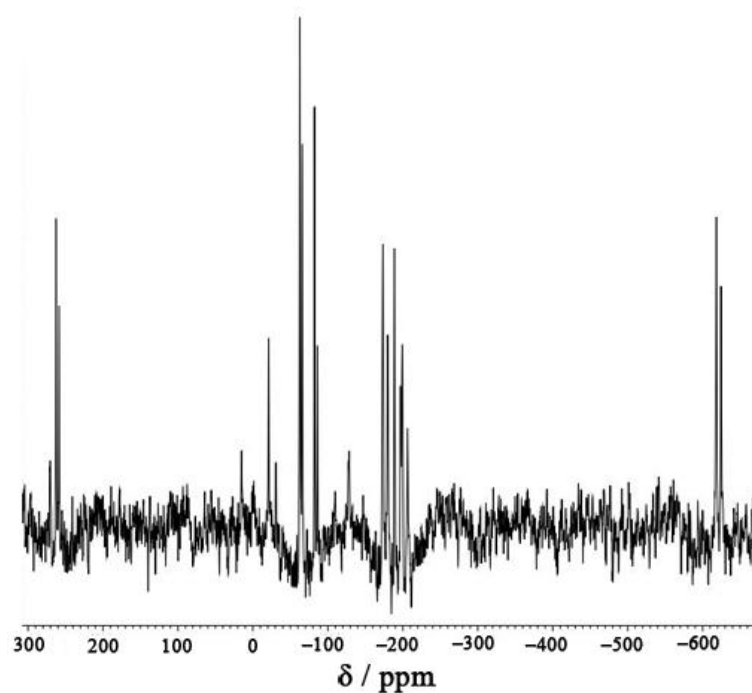


Fig. S7 ^{183}W NMR spectra of **1**

Electrospray ionization mass spectrometry (ESI-MS)

The ESI-MS spectra of compounds **1** and **2** are very similar in their spectral features such as peak shape, position, charge states and so forth.

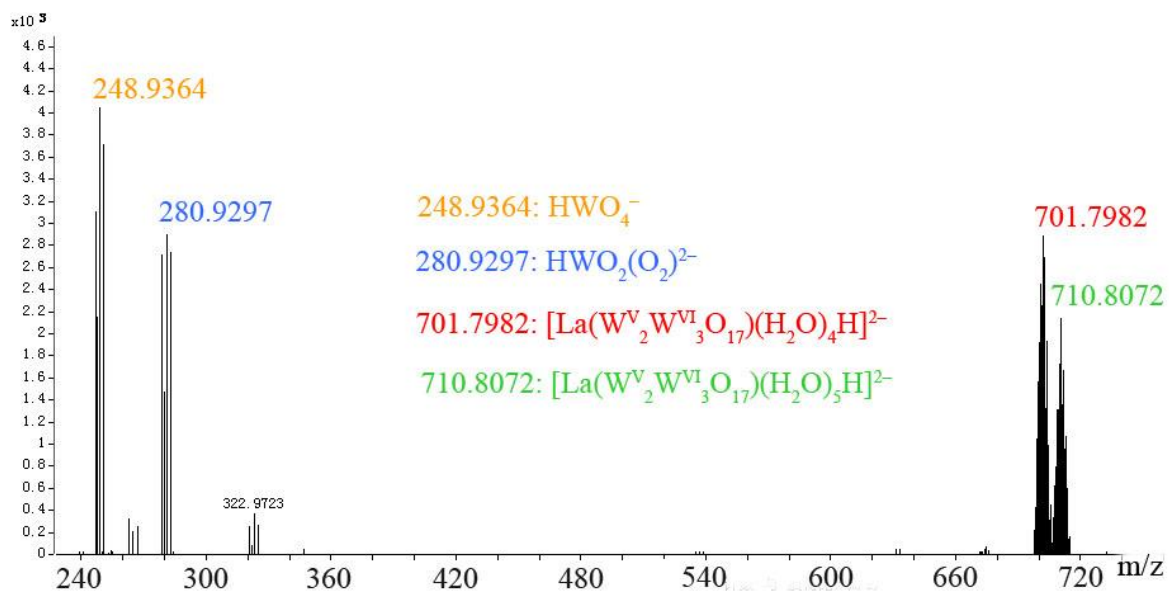


Fig. S8 The negative-mode ESI mass spectrum in water solution of **1** in the $m/z=230-940$ range

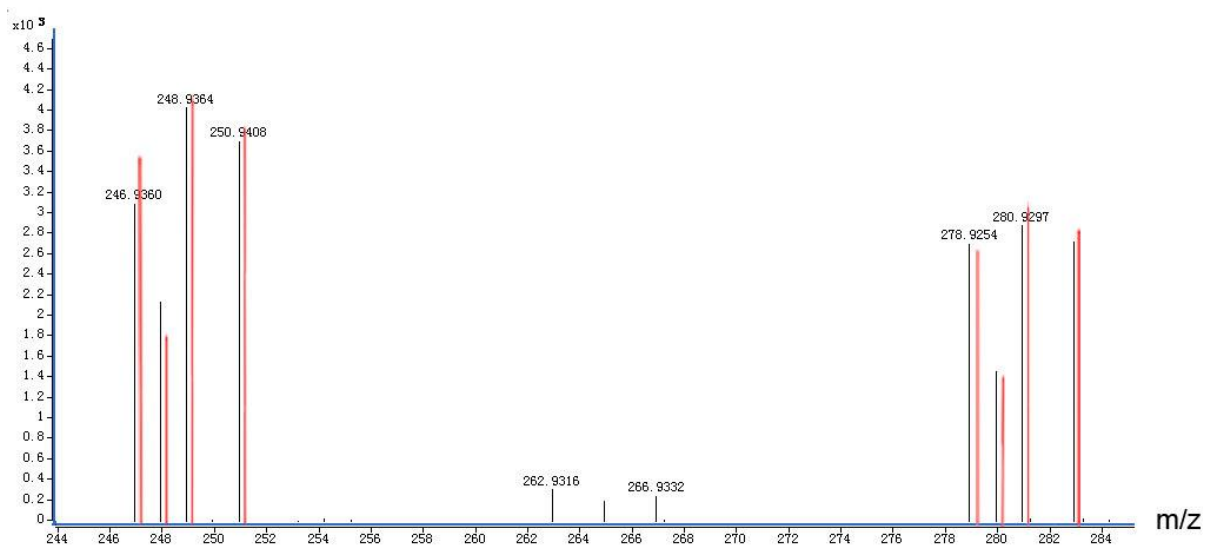


Fig. S9 An expansion of the peaks at m/z 248.9364 (HWO_4^-) and at m/z 280.9297 ($[\text{W}^{\text{VI}}\text{O}(\text{O}_2)_2(\text{OH})]^-$) are shown along with the calculated isotopic pattern (red columns) of **1a**.

Table S7. Calculated isotopic pattern of HWO_4^- (m/z 248.9364)

246.9362	85.82
247.9383	46.48
248.939	100
249.9428	0.54
250.9424	92.88
251.9468	0.15
252.9466	0.76

Table S8. Calculated isotopic pattern of $[\text{W}^{\text{VI}}\text{O}(\text{O}_2)_2(\text{OH})]^-$ (m/z 280.9297)

278.9261	85.49
279.9281	46.36
280.9288	100
281.9326	0.81
282.9322	92.93
283.9365	0.23
284.9365	1.14

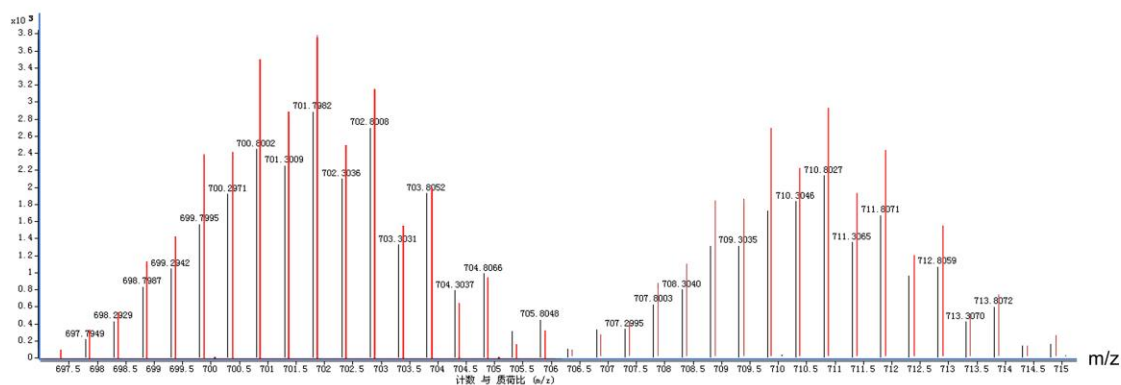


Fig. S10 An expansion of the peaks at m/z 701.7982 ($[\text{La}(\text{W}^{\text{V}}_2\text{W}^{\text{VI}}_3\text{O}_{17})(\text{H}_2\text{O})_4\text{H}]^{2-}$) and at m/z 710.8072 ($[\text{La}(\text{W}^{\text{V}}_2\text{W}^{\text{VI}}_3\text{O}_{17})(\text{H}_2\text{O})_5\text{H}]^{2-}$) are shown along with the calculated isotopic pattern (red columns) of **1a**.

Table S9. Calculated isotopic pattern of $[\text{La}(\text{W}^{\text{V}}_2\text{W}^{\text{VI}}_3\text{O}_{17})(\text{H}_2\text{O})_4\text{H}]^{2-}$ (m/z 701.7982)

697.8077	8.91
698.3085	14.27
698.8091	29.61
699.31	37.29
699.8106	62.46
700.3115	63.25
700.8121	91.5
701.313	75.59
701.8136	100
702.3145	65.31
702.8151	82.49
703.3161	40.71
703.8166	52.42
704.3177	17.15
704.8182	24.82
705.3195	4.39
705.8198	8.5

Table S10. Calculated isotopic pattern of $[\text{La}(\text{W}^{\text{V}}_2\text{W}^{\text{VI}}_3\text{O}_{17})(\text{H}_2\text{O})_5\text{H}]^{2-}$ (m/z 710.8072)

706.813	8.89
707.3138	14.24
707.8144	29.57
708.3153	37.25
708.8159	62.4
709.3168	63.22

709.8174	91.45
710.3183	75.6
710.8189	100
711.3198	65.37
711.8204	82.55
712.3214	40.8
712.8219	52.49
713.323	17.23
713.8235	24.88
714.3248	4.43
714.8251	8.54

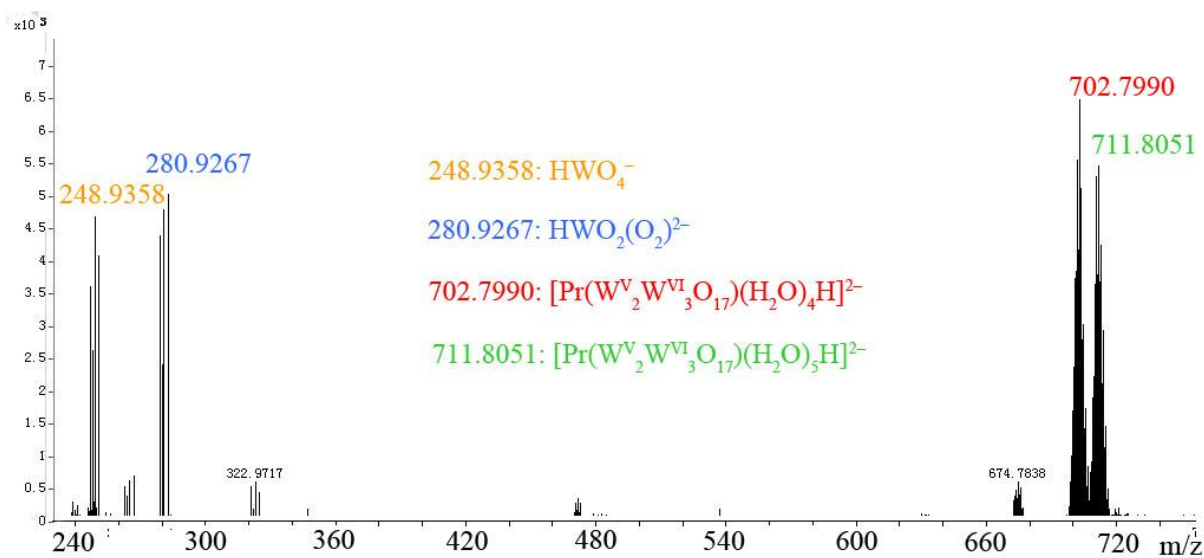


Fig. S11 The negative-mode ESI mass spectrum in water solution of **2** in the $m/z=230-940$ range

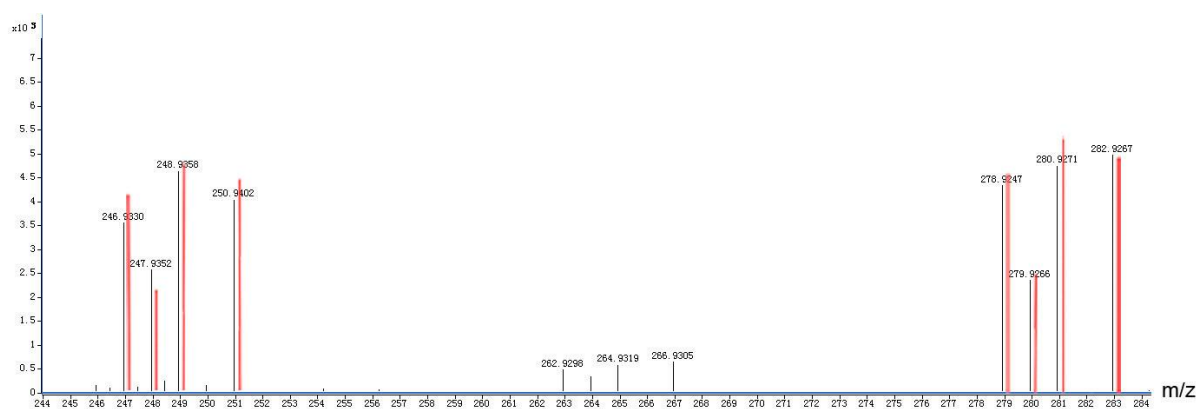


Fig. S12 An expansion of the peaks at m/z 248.9358 (HWO_4^-) and at m/z 280.9271 ($[\text{W}^{\text{VI}}\text{O}(\text{O}_2)_2(\text{OH})]^-$) are shown along with the calculated isotopic pattern (red columns) of **2a**.

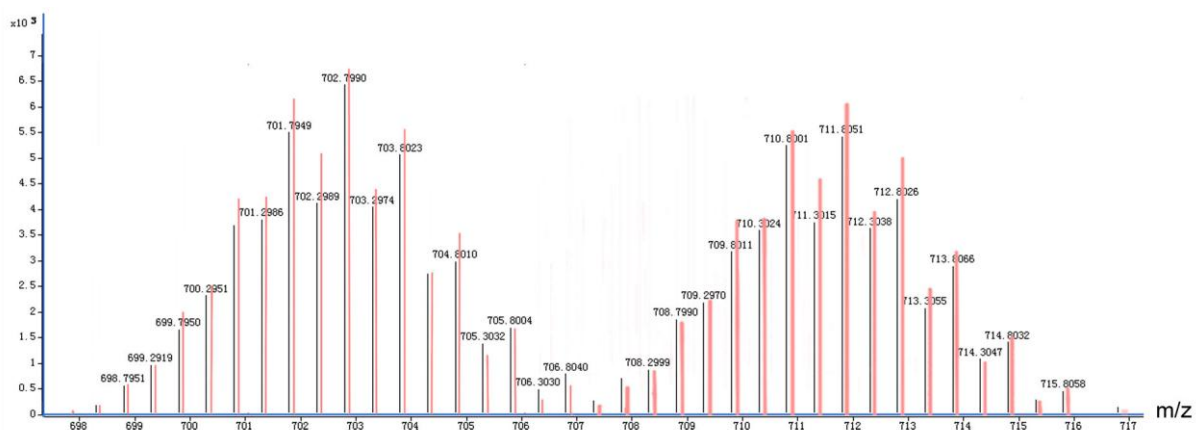


Fig. S13 An expansion of the peaks at m/z 702.7990 ($[\text{Pr}(\text{W}^{\text{V}}_2\text{W}^{\text{VI}}_3\text{O}_{17})(\text{H}_2\text{O})_4\text{H}]^{2-}$) and at m/z 711.8051 ($[\text{Pr}(\text{W}^{\text{V}}_2\text{W}^{\text{VI}}_3\text{O}_{17})(\text{H}_2\text{O})_5\text{H}]^{2-}$) are shown along with the calculated isotopic pattern (red columns) of **2a**.

Table S11. Calculated isotopic pattern of $[\text{Pr}(\text{W}^{\text{V}}_2\text{W}^{\text{VI}}_3\text{O}_{17})(\text{H}_2\text{O})_4\text{H}]^{2-}$ (m/z 702.7990)

699.3092	14.25
699.8098	29.6
700.3106	37.26
700.8112	62.44
701.3121	63.21
701.8127	91.48
702.3137	75.55
702.8142	100
703.3152	65.27
703.8157	82.51
704.3168	40.68
704.8173	52.44
705.3184	17.14
705.8188	24.83

Table S12. Calculated isotopic pattern of $[\text{Pr}(\text{W}^{\text{V}}_2\text{W}^{\text{VI}}_3\text{O}_{17})(\text{H}_2\text{O})_5\text{H}]^{2-}$ (m/z 711.8051)

707.8136	8.88
708.3145	14.22
708.8151	29.56
709.3159	37.22
709.8165	62.38
710.3174	63.17
710.818	91.43

711.3189	75.55
711.8195	100
712.3205	65.34
712.821	82.56
713.3221	40.77
713.8226	52.51
714.3237	17.21
714.8241	24.89

IR spectra

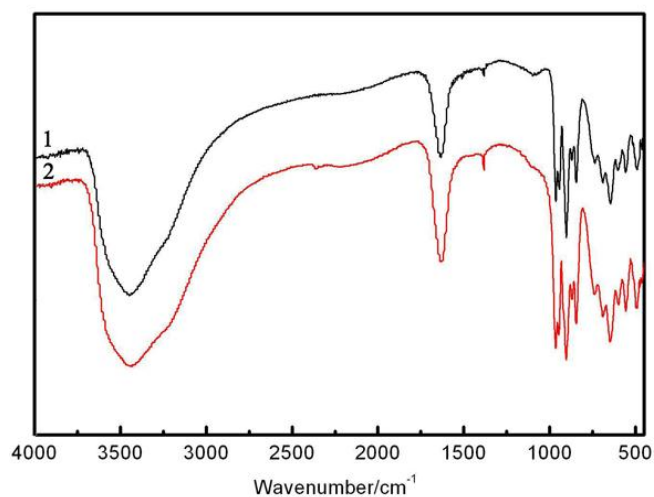


Fig. S14 IR spectra of 1 and 2

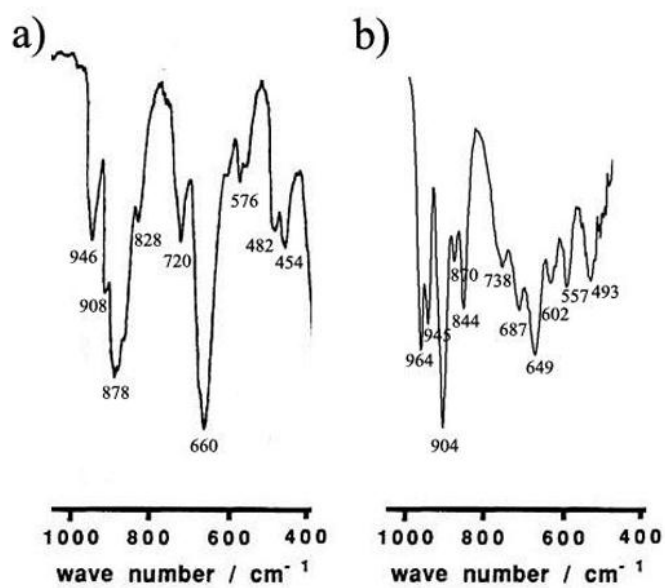


Fig. S15 IR spectra of a) [(t-C₄H₉)NH₃]₆[W₇O₂₄]·2H₂O and b) 2

The IR spectra of **1** and **2** (Fig. S14) show similar features for the skeletal vibrations in the region between 500 and 1000 cm^{-1} , indicating the structural type of the polyoxoanions in **1** and **2** are almost the same, which are in good agreement with the results of single-crystal X-ray structural analysis. Comparing the low-wavenumber region ($\nu < 1000 \text{ cm}^{-1}$) of compound **2** with that of $[\text{W}_7\text{O}_{24}]^{6-}$ ⁸ (Fig. S15). The vibration peak of $\nu_{\text{as}}(\text{W}-\text{O}_i)$ for $[\text{W}_7\text{O}_{24}]^{6-}$ at 946 cm^{-1} is split into two peaks at 964 and 945 cm^{-1} for **2**. The possible major reason for which may be that the Pr^{III} coordinate to the terminal oxygen atoms of the $[\text{W}_7\text{O}_{22}(\text{O}_2)_2]^{6-}$. However, for **2**, in the region between 500 and 900 cm^{-1} , the peaks appear at slightly different frequencies to those found for $[\text{W}_7\text{O}_{22}(\text{O}_2)_2]^{6-}$, for example, 908 cm^{-1} is getting strong and 660 cm^{-1} is getting weak. Two other characteristic vibration bands assigned to $\nu(\text{W}-\mu_2-\text{O}_b)$ and $\nu(\text{W}-\mu_3-\text{O}_b)$ appear at 904 and 870 cm^{-1} for **2**. In addition, the band at 844 cm^{-1} is probably assigned to as $\nu(\text{O}-\text{O})$, and the resonances at 602 cm^{-1} and 557 cm^{-1} may be confidently assigned to the $\nu_{\text{asym}}[\text{W}(\text{O}_2)]$ and $\nu_{\text{sym}}[\text{W}(\text{O}_2)]$ vibration, respectively.⁹⁻¹⁰

X-ray powder diffraction

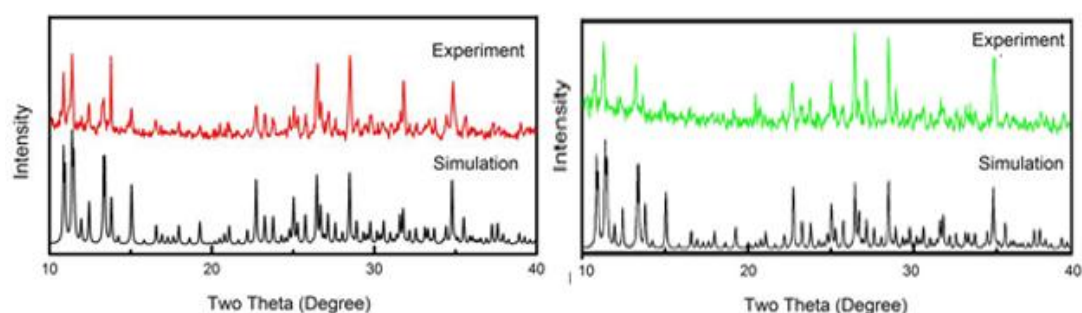


Fig. S16 The simulated and experimental powder XRD pattern of the bulk products **1** (left) and **2** (right).

Simulation based on the single crystal X-ray diffraction data

Two powder X-ray diffraction patterns of **1** and **2** are in good agreement with the calculated patterns based on the results from single-crystal X-ray diffraction (Fig. S16), which confirm that both phases are pure.

References:

- 1 L. Pettersson, I. Andersson and O. W. Howarth, *Inorg. Chem.*, 1992, **31**, 4032.
- 2 C. Streb, C. Ritchie, D. L. Long, P. Kögerler and L. Cronin, *Angew. Chem.* 2007, **119**, 7723; *Angew. Chem. Int. Ed.* 2007, **46**, 7579.
- 3 S. T. Zheng, J. Zhang, J. M. Clemente-Juan, D. Q. Yuan and G. Y. Yang, *Angew. Chem.* 2009, **121**, 7312; *Angew. Chem. Int. Ed.* 2009, **48**, 7104.
- 4 Z. Y. Zhang, Q. P. Lin, S. T. Zheng, X. H. Bu and P. Y. Feng, *Chem. Commun.* 2011, **47**, 3918.
- 5 R. C. Howell, F. G. Perez, S. Jain, W. D. Horrocks, A. L. Rheingold and L. C. Francesconi, *Angew. Chem. Int. Ed.*, 2001, **40**, 4031.
- 6 L. Bi, F. Hussain, U. Kortz, M. Sadakane and M. H. Dickman, *Chem. Commun.*, 2004, **12**, 1420.
- 7 J. Y. Niu, P. T. Ma, H. Y. Niu, J. Li, J. W. Zhao, Y. Song and J. P. Wang, *Chem. Eur. J.* 2007, **13**, 8739.
- 8 S. Ikenoue¹, M. Mikuriya¹, O. Miyauchi¹, R. Nukada¹ and A. Yagasaki¹, *Bulletin of the Chemical Society of Japan*, 1994, **67**, 2590.
- 9 J. Y. Piquemal, L. Salles, G. Chottard, P. Herson, C. Ahcine and J. M. Brégeault, *Eur. J. Inorg. Chem.* 2006, **5**, 939.
- 10 J. S. Carrió, J. B. Serra, M. E. G. Núñez, A. G. Gastaldi, G. B. Jameson, L. C. W. Baker and R. Acerete, *J. Am. Chem. Soc.*, 1999, **121**, 977.